Vibration Control of a PZT Actuated Suspension Dual-Stage Servo System Using a PZT Sensor

Yunfeng Li, Roberto Horowitz, and Robert Evans

***Abstract*—Structural resonance modes of the head stack and suspension assembly are one of the major limiting factors for achieving higher head-positioning servo performance in hard disk drives. This paper discusses the vibration suppression control of a PZT actuated suspension dual-stage servo system. A PZT strip on a PZT actuated suspension is utilized as a vibration sensor to control both the voice coil motor (VCM) actuator butterfly mode and the suspension sway mode. The vibration suppression controller is designed using the H_∞ control design method. Experimental results show that an attenuation of 15 dB can be achieved for both the suspension sway mode and the VCM butterfly mode, and the rms of the head off-track motion due to airflow excited vibration can be reduced by approximately 30% with the proposed vibration suppression control scheme.**

***Index Terms*—Dual-stage servo, hard disk drive, vibration damping control, windage.**

I. Introduction

STRUCTURAL resonance modes of the head stack and suspension assembly are one of the major limiting factors for achieving higher head-positioning servo performance in hard disk drives. These lightly damped resonance modes can be excited by airflow generated from disk rotation and other disturbances and cause head off-track motion. They also limit the achievable servo bandwidth of the track-following servo system. Active control of these vibration modes requires a very high bandwidth and sampling frequency. However, the sampling frequency of the position error signal (PES) is limited by the number of servo sectors allocated to store position information on a data track. Several researchers have proposed to incorporate additional vibration sensors to control structural vibration modes [1]–[3]. For example, it has been shown that the butterfly mode can be damped with a feedback damping control loop by attaching a strain sensor on the E-block near the pivot [2].

PZT actuated suspensions have been developed as the first generation second-stage actuators for dual-stage actuation in disk drive servo. The PZT actuators, placed near the root of the suspension, generate a push–pull action that displaces the head, which is located at the tip of the suspension. In order to increase the actuation gain from the actuator to the head lateral motion and reduce the driving voltage, PZT actuated suspensions are usually designed to have a relatively low-frequency sway mode. This makes these suspensions more susceptible to airflow excitations than their conventional counterparts. To solve this problem, a control scheme to damp the suspension sway mode, by utilizing one of the two PZT strips as a vibration sensor and the other one as an actuator, has been proposed [3]. The tests in [3] were conducted using a single PZT actuated suspension mounted on a spin stand. In this paper, the active vibration control of a PZT actuated suspension dual-stage actuator using similar techniques is presented. A vibration damping controller has been designed and tested to actively damp the head stack assembly butterfly mode and the suspension sway mode, by using the output of the PZT sensor and the dual-stage actuator. Section II discusses the use of the frequency response peak-amplitude method to identify a model of the control system. Section III discusses damping controller design using the H_∞ control design method. Experimental results are presented and discussed in Section IV, and conclusions are given in Section V.

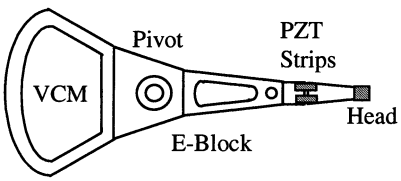

Fig. 1. PZT actuated suspension dual-stage actuator.

II. Modelling of the Sensor and the Actuator

Fig. 1 shows a diagram of a PZT actuated suspension dual-stage actuator. It consists of the voice coil motor (VCM), pivot bearing, and E-block as the primary stage actuator and a PZT actuated suspension as the second stage actuator. As shown in the figure, the PZT actuated suspension has two PZT strips located near the root of the suspension, which generate a push–pull action to actuate the head located at the tip of the suspension. When a mechanical stress is applied to a piezoelectric material, such as PZT, it will generate charge. Thus, the PZT element can also be used as a strain sensor. In this paper, one PZT strip on the suspension is used as a vibration sensor, and the other strip is used as an actuator. The control system being considered is a two-input two-output control system. The two inputs are inputs to the VCM and the PZT actuator. The two outputs are the head displacement and the PZT sensor output.

Manuscript received July 16, 2002. This work was supported in part by a gift from the Information Storage Industry Consortium (INSIC) and a grant from the Computer Mechanics Laboratory (CML) at U.C. Berkeley.

Y. Li and R. Horowitz are with the Department of Mechanical Engineering, University of California, Berkeley, CA 94720-1740 USA (e-mail: yunfeng@me.berkeley.edu; horowitz@me.berkeley.edu).

R. Evans is with Hutchinson Technology Incorporated, Hutchinson, MN 55350 USA (e-mail: Robert.Evans@hti.htch.com).

Digital Object Identifier 10.1109/TMAG.2003.808952

0018-9464/03$17.00 © 2003 IEEE

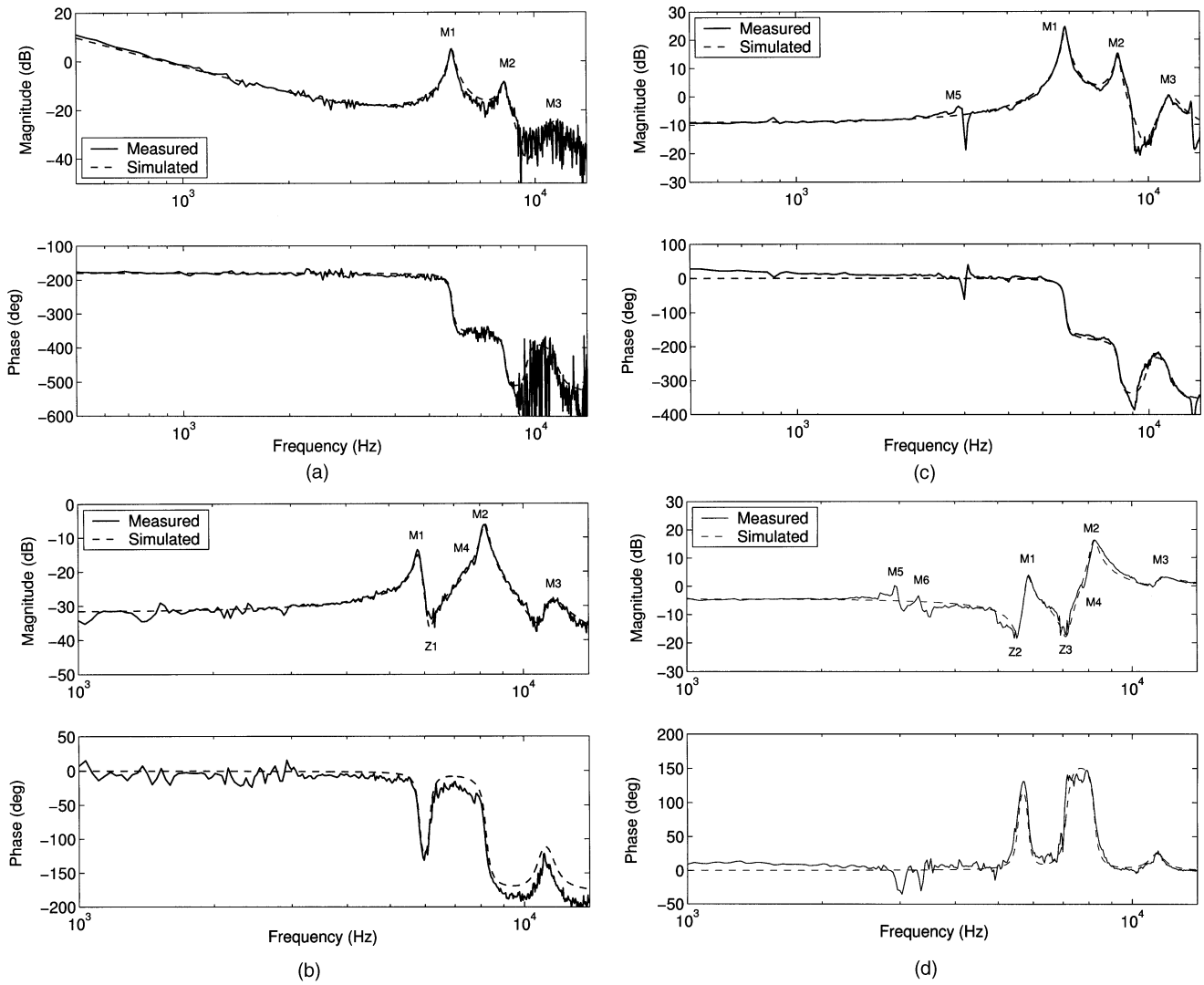

Fig. 2. Frequency responses: (a) from VCM input to head displacement, (b) from PZT actuator input to head displacement, (c) from VCM input to PZT sensor output, and (d) from PZT actuator input to PZT sensor output.

A. Frequency Response of the Sensor and the Actuator

Let u_1 and u_2 be the inputs to the VCM and the PZT actuator, respectively, and y_1 and y_2 be the head displacement output and the PZT vibration sensor output, respectively. The plant transfer function from u_j to y_i, $G_{ij}(s)$, $i, j = 1, 2$, can be written as

$$G_{ij}(s) = \frac{A_0^{ij}}{s^2} + \sum_{n=1}^{N} \frac{\omega_n^2 A_n^{ij}}{s^2 + 2\zeta_n \omega_n s + \omega_n^2} + d_{ij} \qquad (1)$$

which is a summation of the rigid body mode, a number of structural vibration modes, and a direct feeding term from the input to the output. In (1), A_0^{ij} is the gain of the rigid body mode, N is the total number of vibration modes being considered, ω_n and ζ_n are the natural frequency and damping ratio of mode n respectively, A_n^{ij} is the modal constant of mode n, and d_{ij} is the direct feedthrough factor from u_j to y_i.

Fig. 2 shows the following measured and modeled frequency responses: 1) from VCM input (u_1) to head displacement (y_1); 2) from PZT actuator input (u_2) to head displacement (y_1); 3) from VCM input (u_1) to PZT sensor output (y_2); and 4) from PZT actuator input (u_2) to PZT sensor output (y_2). The head displacement was measured using a laser Doppler vibrometer (LDV). The solid lines in the figures are the experimental data, while dashed lines are the simulated results using the identified model. The major identified vibration modes in the figures include the VCM actuator butterfly mode (M1), the suspension sway mode (M2), the suspension second torsion mode (M3), and the suspension first torsion mode (M4). In the butterfly mode, which is generated from the coupling of the in-plane sway modes of the E-block arm and the coil, the arm and the coil move out of phase around the pivot. The suspension sway mode is also called the actuation mode of the PZT actuator.

As shown in Fig. 2(a), the VCM actuator frequency response is dominated by the rigid body mode in the low frequency range. The major off-track vibration modes excited by the VCM are the butterfly mode and the suspension sway mode (M1 and M2).

As shown in Fig. 2(b), the biggest peak of the PZT actuator frequency response is the suspension sway mode (M2). The butterfly mode (M1) also appears as a reaction mode in this frequency response because it is excited by the PZT actuator, through the swage connection between the suspension and the E-block arm. The PZT actuator frequency response is almost flat

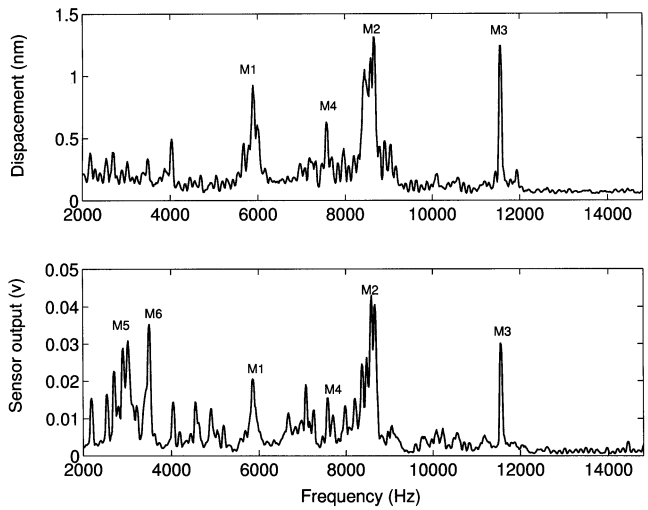

Fig. 3. PSDs of the head off-track motion and the PZT sensor output.

at low frequency, which implies that the excitation of the rigid body mode by the PZT actuator is negligible, since the torque generated by the PZT actuator is small compared to the inertia of the head stack assembly. The coupling between the butterfly mode and the suspension sway mode results in a pair of lightly damped zeros (Z1), which follow the poles of the butterfly mode (M1) in the frequency response.

Fig. 2(c) and (d) shows the frequency responses of the PZT sensor output. It should be emphasized that the two PZT strips on the PZT actuated suspension were not designed to be sensors, but actuators, and their locations have not been optimized for vibration sensing. Thus, even though one of them can be used as a vibration sensor, its performance may not be optimal. As a consequence, it may not be able to sense the vibration of some off-track modes, while senses the vibration of some nonoff-track modes. Fortunately, as shown in Fig. 2(c) and (d), it seems that the PZT sensor is able to pick up most of the off-track modes. However, it also picks up some of the nonoff-track modes [M5 and M6 in Fig. 2(c) and (d)].

B. Airflow Excited Actuator Vibration

Fig. 3 shows the power spectrum densities (PSDs) of the head off-track motion (upper half) and the PZT sensor output (bottom half) when the spindle is rotating in a 7200 rpm disk drive and no control is applied. As shown in the figure, the major off-track modes excited by the airflow generated by disk rotation include the butterfly mode (M1), the suspension sway mode (M2), the suspension second torsion mode (M3), and the suspension first torsion mode (M4). The PZT sensor is able to sense the vibration of modes M1, M2, and M3. However, it barely picks up the vibration of the suspension first torsion mode (M4), as it is being excited by the airflow. Modes M5 and M6 are also excited by the airflow and have big contributions to the PZT sensor output, yet they have little contributions to the head off-track motion. They will act as sensor unmodeled dynamics and must be properly compensated for in the controller design.

C. Modal Parameters Extraction Using Modal Testing

The modal parameters, ζ_n, ω_n, A_n^{ij}, $n = 1, \ldots, N$, $i, j = 1, 2$, in (1) can be extracted from the measured frequency responses. If the resonance frequencies of those modes are not closely spaced, and the modes are lightly damped, the modal parameters of each mode can be estimated separately using a single-degree-of-freedom (SDOF) modal testing method, such as the peak-magnitude method or circle-fit method. Under these conditions, the response near each resonance frequency is dominated by just one mode, and the effects due to the other modes can be neglected [4]. Preliminary examination of the frequency responses in Fig. 2 shows that the major resonance modes are indeed spaced apart and are lightly damped. Thus, a simple SDOF modal testing method could be used to estimate the modal parameters.

TABLE I
EXTRACTED MODAL PARAMETERS

Parameters	Mode 1	Mode 2	Mode 3
ω (Hz)	5830	8220	11500
ζ	0.015	0.018	0.05
A^{11}	-0.056	0.014	0.006
A^{12}	0.005	0.018	0.003
A^{21}	-0.45	0.18	0.1
A^{22}	0.04	0.23	0.05

In the peak-magnitude method [4], the resonance frequency is first obtained by examining local resonance peaks. For a lightly damped resonance mode, the natural frequency ω is approximately equal to the resonance frequency ω_r

$$\omega \approx \omega_r. \tag{2}$$

The damping ratio can be estimated from the so-called "half-power" or "-3 dB-magnitude" points by

$$\zeta \approx \frac{\omega_a - \omega_b}{2\omega_r} \tag{3}$$

where ω_a and ω_b are the frequencies at which the magnitude of the frequency response is $1/\sqrt{2}$ of the peak magnitude at the resonance frequency. The modal constant can then be estimated by

$$A \approx 2H_r\zeta \tag{4}$$

where H_r is the peak magnitude of the frequency response at the resonance frequency.

Three modes, the butterfly mode (M1), the suspension sway mode (M2), and the suspension second torsion mode (M3), were included in the modal analysis. First, natural frequencies, ω_n, and damping ratios, ζ_n, were estimated by using (2) and (3) based on the measured frequency response from the PZT actuator to the head displacement, as shown in Fig. 2(b), which is the cleanest of the four measured frequency responses in Fig. 2.

Next, modal constants A_n^{11}, A_n^{12}, A_n^{21}, and A_n^{22} were estimated. Note that only three of the four model constants are independent. The last three were estimated by using (4) based on the measured frequency responses in Fig. 2(b)–(d). A_n^{11} was calculated by

$$A_n^{11} = \frac{A_n^{21} * A_n^{12}}{A_n^{22}}, \quad n = 1, 2, 3. \tag{5}$$

Table I lists all modal parameters extracted using this method.

The feedthrough term d_{ij} can be estimated by matching the dc gains of the measured frequency responses. The feedthrough terms from u_1 and u_2 to the head displacement y_1 were found to be $d^{11} = 0$, $d^{12} = 0$, as expected. The feedthrough terms from u_1 and u_2 to the PZT sensor output y_2 were found to be $d^{21} = -0.18$, $d^{22} = -0.92$. They are not zero because there exists some direct structural connection path from the actuators to the sensor. The feedthrough terms coupled with other vibration modes produce zeros in the transfer functions $G_{21}(s)$ and $G_{22}(s)$ in (1), as shown in the frequency responses in Fig. 2(c) and (d).

D. A State Space Model

The control system can be represented using a state-space model based on the transfer functions in (1) and the parameters in Table I. The rigid body mode is not observable from the PZT sensor output and is not of interest in designing vibration suppression controllers. Thus, it is not included in the state-space model. A state space realization including the three vibration modes (M1, M2, M3) is

$$\dot{\mathbf{x}} = \mathbf{A}\mathbf{x} + \mathbf{B}\mathbf{u} \tag{6}$$

$$\mathbf{y} = \mathbf{C}\mathbf{x} + \mathbf{D}\mathbf{u} \tag{7}$$

where $\mathbf{x} = [x_1 \quad x_2 \quad x_3 \quad x_4 \quad x_5 \quad x_6]^T$, $\mathbf{u} = [u_1 \quad u_2]^T$, $\mathbf{y} = [y_1 \quad y_2]^T$, and the state matrices can be written as

$$\mathbf{A} = \begin{bmatrix} 0 & 1 & 0 & 0 & 0 & 0 \\ a_{11} & a_{12} & 0 & 0 & 0 & 0 \\ 0 & 0 & 0 & 1 & 0 & 0 \\ 0 & 0 & a_{21} & a_{22} & 0 & 0 \\ 0 & 0 & 0 & 0 & 0 & 1 \\ 0 & 0 & 0 & 0 & a_{31} & a_{32} \end{bmatrix}$$

$$\mathbf{B} = \begin{bmatrix} 0 & 0 \\ b_{11} & b_{12} \\ 0 & 0 \\ b_{21} & b_{22} \\ 0 & 0 \\ b_{31} & b_{32} \end{bmatrix}$$

$$\mathbf{C} = \begin{bmatrix} c_{11} & 0 & c_{12} & 0 & c_{13} & 0 \\ c_{21} & 0 & c_{22} & 0 & c_{23} & 0 \end{bmatrix}$$

$$\mathbf{D} = \begin{bmatrix} d_{11} & d_{12} \\ d_{21} & d_{22} \end{bmatrix}$$

and

$$a_{n1} = -\omega_n^2, \quad a_{n2} = -2\zeta_n\omega_n, \quad n = 1, 2, 3. \tag{8}$$

By normalizing the PZT sensor output equation with $c_{2n} = 1$, $n = 1, 2, 3$, the other coefficients can be given by

$$b_{n1} = A_n^{21} \tag{9}$$

$$b_{n2} = A_n^{22} \tag{10}$$

$$c_{1n} = \frac{A_n^{11}}{A_n^{21}} = \frac{A_n^{12}}{A_n^{22}} \tag{11}$$

where $n = 1, 2, 3$.

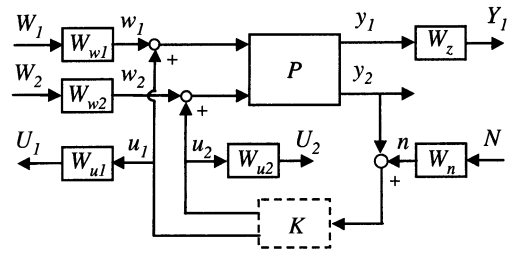

Fig. 4. H_∞-controller design block diagram.

III. Vibration Suppression Controller Design

For a single-input/single-output system, two classical active damping control techniques have been widely used in practice to actively damp a single resonance mode [5]. The first one is to use velocity negative feedback (or lead compensation) accompanied by the use of a low-pass filter. The second one is to use positive position feedback, accompanied by a second-order low-pass filter with the same natural frequency as that of the mode being damped. Both damping control techniques rely on an approximately $+90^\circ$ phase lead contribution from the controller to make the phase of the open loop system close to 0° at the resonance frequency of the mode being damped.

For a multi-input multi-output system, the controller can be designed using pole placement state feedback control to damp multiple resonance modes. However, this method requires precise modeling of the control system in order to obtain a good state estimator. The use of a reduced-order model with a limited number of modes in state estimation may lead to observability and controllability spillovers, which result in the lack of stability and performance robustness [5].

In this paper, an H_∞-control design technique is used to design the vibration damping controller. A block diagram for the H_∞-controller design is shown in Fig. 4. In the block diagram, P represents the two-input two-output plant, which is described by the state and output equations in (6)–(11); K is the controller to be synthesized, u_1 and u_2 are the control inputs to the VCM and PZT actuator respectively, w_1 and w_2 are disturbances, n is the sensor measurement noise, y_1 is the head displacement (excluding the rigid body mode), and y_2 is the PZT sensor output. Note that the only input to the damping controller is the PZT sensor output. Thus, the control sampling frequency is not limited by the PES sample rate.

W_{u1}, W_{u2} , W_{w1}, W_{w2}, W_n, and W_{y1} in the block diagram are weighting functions, which must be selected to characterize the disturbances and design objectives. W_{w1}, W_{w2}, and W_{y1} are constant weights selected to bound the peak magnitude of the closed loop frequency responses. W_{w1} and W_{w2} were chosen to be

$$W_{w1} = \frac{1}{g_{\text{vcm}}}, \quad W_{w1} = \frac{1}{g_{\text{pzt}}} \tag{12}$$

respectively, where g_{vcm} and g_{pzt} are the dc gains of the VCM and the PZT actuator, respectively. W_{y1} was chosen to equal 4 (or 12 dB), which bounds the closed loop resonance peaks of the VCM and the PZT actuator to be within 12 dB.

W_n was chosen to be a "base-shape" filter, since the PZT sensor picks up some high-order modes in the high-frequency

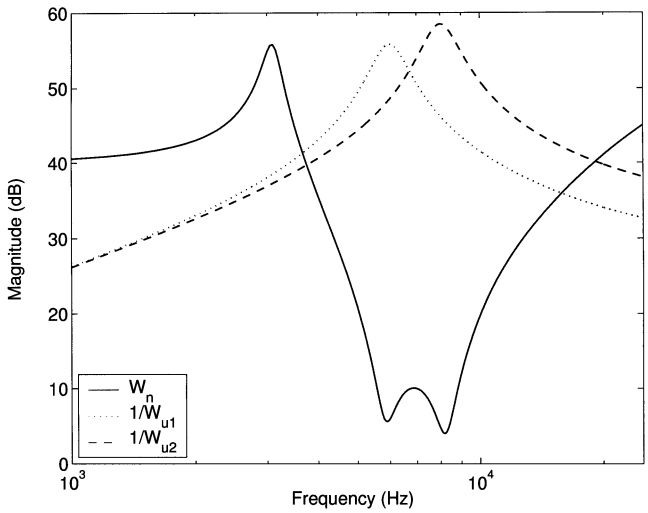

Fig. 5. Magnitude plots of weighting function W_n, W_{u1}, and W_{u2}.

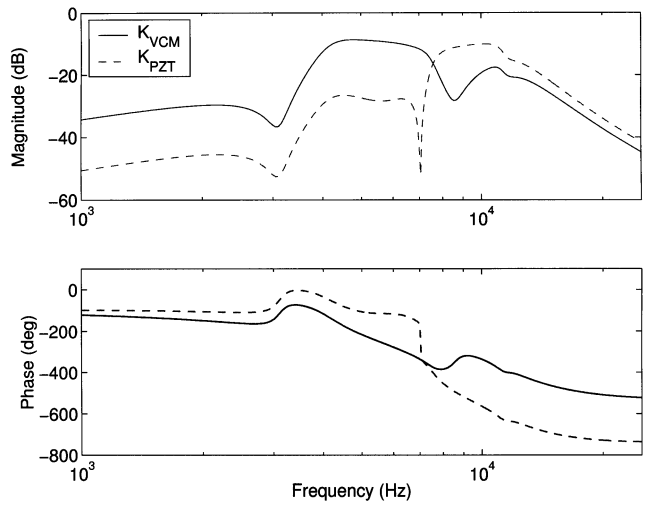

Fig. 6. Bode plots of the synthesized damping controllers.

range, which have little off-track contribution, while in the low-frequency range, it picks up the disturbances at harmonics of the spindle rotation frequency. The transfer function of $W_n(s)$ was selected to be

$$W_n(s) = 100 \left(\frac{\frac{s^2}{\omega_{nz1}^2} + \frac{2\zeta_{nz1}s}{\omega_{nz1}} + 1}{\frac{s^2}{\omega_{np1}^2} + \frac{2\zeta_{np1}s}{\omega_{np1}} + 1} \right) \cdot \left(\frac{\frac{s^2}{\omega_{nz2}^2} + \frac{2\zeta_{nz2}s}{\omega_{nz2}} + 1}{\frac{s^2}{\omega_{np2}^2} + \frac{2\zeta_{np2}s}{\omega_{np2}} + 1} \right) \quad (13)$$

where $\omega_{nz1} = 5930 * 2\pi$, $\zeta_{nz1} = 0.1$, $\omega_{np1} = 3100 * 2\pi$, $\zeta_{np1} = 0.1, \omega_{nz2} = 8220*2\pi, \zeta_{nz2} = 0.1, \omega_{np2} = 50\,000*2\pi$, $\zeta_{np1} = 1$. The solid line in Fig. 5 shows the magnitude of the frequency response of $W_n(s)$. The peak near 3.1 kHz is used to represent the nonoff-track modes (M5 and M6) in the PZT sensor output (see Fig. 3).

The control signal weights W_{u1} and W_{u2} were designed to be

$$W_{u1}(s) = 0.05 \left(\frac{\left(\frac{s}{\omega_{uz1}} + 1\right)\left(\frac{s}{\omega_{uz2}} + 1\right)}{\frac{s^2}{w_{up1}^2} + \frac{2*0.1s}{w_{up1}} + 1} \right) \quad (14)$$

$$W_{u2}(s) = 0.05 \left(\frac{\left(\frac{s}{\omega_{uz1}} + 1\right)\left(\frac{s}{\omega_{uz1}} + 1\right)}{\frac{s^2}{w_{up2}^2} + \frac{2*0.1s}{w_{up2}} + 1} \right) \quad (15)$$

respectively, where $\omega_{uz1} = 50*2\pi, \omega_{uz1} = 25\,000*2\pi, \omega_{up1} = 6000 * 2\pi$, $\zeta_{up1} = 0.1, \omega_{up2} = 8000 * 2\pi$, $\zeta_{up2} = 0.1$. The dot and dash lines in Fig. 5 show the magnitude of the frequency responses of $1/W_{u1}$ and $1/W_{u2}$, respectively. They shape the control actions to be like lead compensation cascaded with low pass filters.

The combination of W_{u1}, W_{u2}, and W_n described above makes the synthesized controllers have small gains in the frequency ranges below 3 and above 8 kHz, and have notches near the nonoff-track sensor noise modes (M5 and M6), as shown in the Bode plots of the synthesized VCM loop controller, $K_{\mathrm{VCM}}(s)$, and the PZT loop controller, $K_{\mathrm{PZT}}(s)$, in Fig. 6. Because of the small gains in the low frequency range, the vibration damping controllers will have little effect on the dynamics and gains of the VCM and PZT actuator for track-following control. They roll-off at high frequency to attenuate high frequency sensor noise.

One important consideration in the controller design of a dual-input control system is that the destructive effect, that occurs when the two actuators fight each other, must be avoided [6]. The weighting functions W_{u1} and W_{u2} designed above also prevent the destructive motion between the VCM and the PZT actuator. As shown in Figs. 5 and 6, $K_{\mathrm{VCM}}(s)$ was designed to have high gain near the butterfly mode frequency and low gain near the suspension sway mode frequency, while $K_{\mathrm{PZT}}(s)$ was designed to have high gain near the suspension sway mode frequency and low gain near the butterfly mode frequency. Thus, the control action of the VCM is primarily used for suppressing butterfly mode vibration, while the control action of the PZT actuator is primarily used for suppressing suspension sway mode vibration. Thus, the destructive motion between the two actuators is prevented.

IV. Experimental Results

Experiments have been conducted using a PZT-actuated suspension dual-stage actuator in a disk drive. The spindle rotation speed is 7200 rpm. The synthesized controller was reduced to seventh order from an initial 14th order and was implemented on a floating point DSP running at 100 kHz sampling frequency. Figs. 7 and 8 show the comparisons of the open-loop and closed-loop frequency responses of the VCM and PZT actuator, respectively. Both the VCM actuator butterfly mode and the suspension sway mode are attenuated by about 15 dB in closed-loop mode. However, the resonance peaks are not entirely flattened out. The active damping control performance is limited by several factors. First, the coupling effects among multiple resonance modes in the sensor output make control design difficult. The controller gain and phase must be carefully tuned to avoid instability. Ideally, multiple sensors could be used to sense each individual resonance mode to be damped, in order to achieve the best performance. Second,

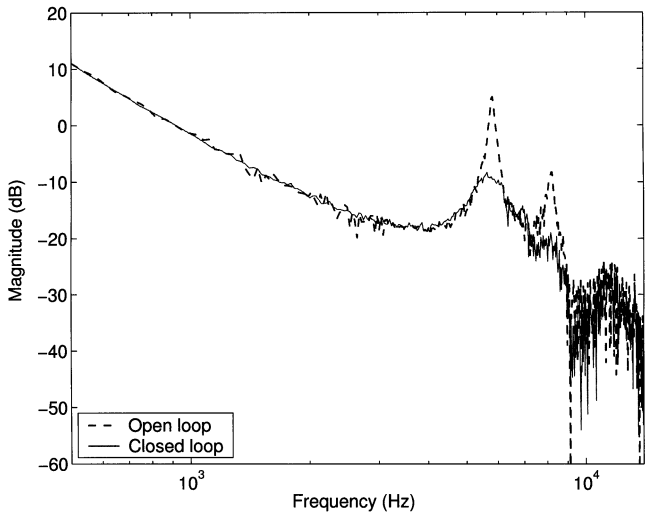

Fig. 7. Closed-loop frequency response of the VCM actuator.

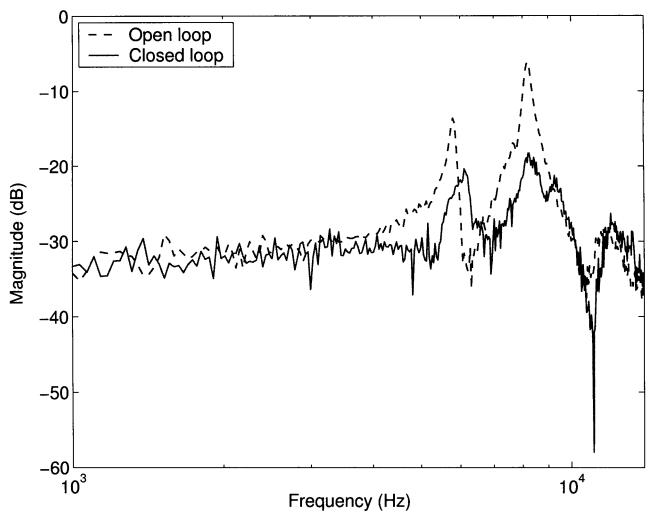

Fig. 8. Closed-loop frequency response of the PZT actuator.

the PZT sensor picks up some nonoff-track modes, which are close in frequency to the vibration modes to be damped. Thus, there is a tradeoff between noise rejection (needing low control gain near the noise modes frequency) and vibration mode suppression (needing high control gain near the resonance frequency of the vibration mode to be damped). Third, the time delay in our experimental setup was relatively long, totalling 17 μs. This results in a phase loss of about 40°–60° near the crossover frequencies. It could cause spillover and mode splitting problems if the control gains are set too high.

Fig. 9 compares the open-loop and closed-loop PSDs of the head off-track motion, as measured by an LDV and a digital spectrum analyzer. The dashed line is the PSD of head motion when damping control is not applied, while the solid line is when damping control is applied. Airflow excited vibrations of modes M1, M2, and M3 are attenuated by the damping controller. Overall, the rms value of the PSD from 2 to 14.8 kHz is reduced by about 30% when vibration control is applied.

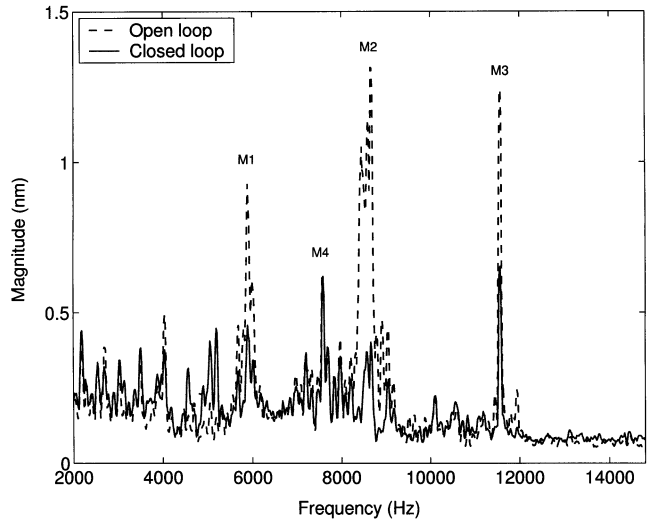

Fig. 9. Power spectrum density of the head motion.

V. Conclusion

The use of one PZT strip as a vibration sensor provides a simple solution to attain vibration suppression control of a PZT-actuated suspension dual-stage servo system. In this paper, a vibration model of the dual-stage actuator was obtained by modal testing, using measured frequency responses. A vibration damping controller was designed using the H_∞ control design methodology. Experimental results show that the proposed control scheme can partially damp the VCM butterfly mode and the suspension sway mode and reduce head off-track motion due to airflow excited vibration. Future works to combine damping control and track-following control will be conducted.

Acknowledgment

The authors would like to thank E. Fanslau, R. Heist, L. Kim, M. McCaslin, and A. Uppal from Read-Rite for their help with the test drive and B. Thornton, H. Gross, and Prof. D. Bogy at CML, UCB, for their help with the experimental setup. They would also like to thank the other members of the INSIC EHDR servo team for their valuable comments, suggestions, and support.

References

[1] Y. Huang, M. Banther, P. Mathur, and W. Messner, "Design and analysis of a high bandwidth disk drive servo system using an instrumented suspension," *IEEE/ASME Trans. Mechatron.*, vol. 4, pp. 196–206, June 1999.

[2] F.-Y. Huang, T. Semba, W. Imaino, and F. Lee, "Active damping in HDD actuator," *IEEE Trans. Magn.*, vol. 37, pp. 847–849, Mar. 2001.

[3] Y. Li and R. Horowitz, "Active vibration control of a PZT actuated suspension in hard disk drives," in *Proc. Amer. Automatic Control Conf.*, Anchorage, Alaska, May 2002.

[4] D. Ewins, *Modal Testing: Theory, Pratice and Application*, 2nd ed. Bladock, Hertfordshire, U.K.: Research Studies Press, 2000.

[5] R. Kashani. (2002) Active vibration damping. [Online]. Available: http://www.deicon.com/vib_tutorial/act_vib2_pdf.pdf

[6] S. Schroeck, W. Messner, and R. McNab, "On compensator design for linear time-invariant dual-input single-output systems," *IEEE/ASME Trans. Mechatron.*, vol. 6, pp. 50–57, Mar. 2001.